Title: Supercritical anti-solvent fractionation of *Artemisia absinthium* L. conventional extracts: tracking artemetin and casticin

Authors: Elisa Langa, Juan I. Pardo, Carlota Giménez-Rota, Azucena González-Coloma, María J. Hernáiz, Ana M. Mainar

PII: S0896-8446(18)30590-4
DOI: https://doi.org/10.1016/j.supflu.2019.05.003
Reference: SUPFLU 4535

To appear in: *J. of Supercritical Fluids*

Received date: 8 September 2018
Revised date: 6 May 2019
Accepted date: 6 May 2019

Please cite this article as: Langa E, Pardo JI, Giménez-Rota C, González-Coloma A, Hernáiz MJ, Mainar AM, Supercritical anti-solvent fractionation of *Artemisia absinthium* L. conventional extracts: tracking artemetin and casticin, *The Journal of Supercritical Fluids* (2019), https://doi.org/10.1016/j.supflu.2019.05.003

Supercritical anti-solvent fractionation of *Artemisia absinthium* L. conventional extracts: tracking artemetin and casticin.

Elisa Langa[a, b], Juan I. Pardo[a], Carlota Giménez-Rota[a], Azucena González-Coloma[c], María J. Hernáiz[d], Ana M. Mainar[a*]

[a] GATHERS Group, Aragón Institute of Engineering Research (I3A), Universidad de Zaragoza, c/. Mariano Esquillor s/n, 50018 Zaragoza, Spain

[b] Universidad San Jorge, Campus Universitario Villanueva de Gállego, Autovía A-23 Zaragoza-Huesca Km. 299, 50830 Villanueva de Gállego (Zaragoza), Spain

[c] Instituto de Ciencias Agrarias, CSIC, C/Serrano 115-bis, 28006 Madrid, Spain

[d] Chemistry in Pharmaceutical Science Department, Pharmacy Faculty, Complutense University of Madrid, Plaza Ramón y Cajal s/n, Madrid 28040, Spain

* Corresponding author: ammainar@unizar.es, phone number: +34976761195

Graphical abstract

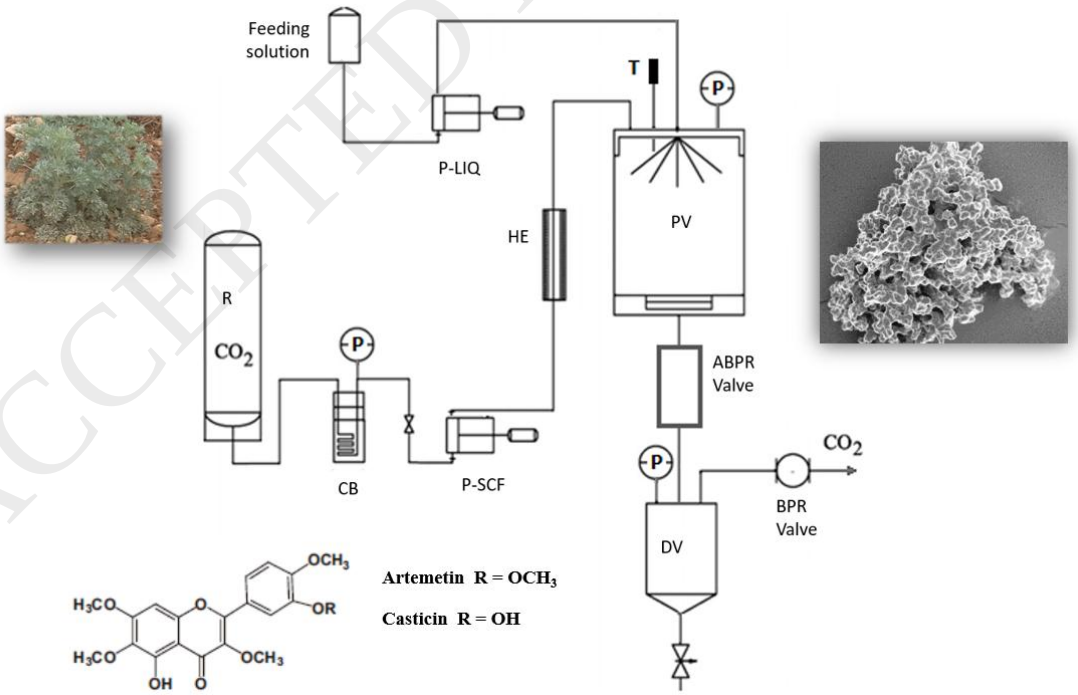

HIGHLIGHTS

- Supercritical anti-solvent fractionation were applied for the first time to *A. absinthium*
- CO_2 pressure and flow rate were modified to get different extract fractions
- Artemetin and casticin were tracked in every experiment
- Fraction enriched in artemetin using supercritical anti-solvent fractionation was obtained

Abstract

In the current work the Supercritical Anti-solvent Fractionation (SAF) methodology was applied to conventional extracts from *Artemisia absinthium* L. (wormwood). Artemetin and casticin, two compounds found in wormwood extracts and with high structural similarity, were tracked in all the experiments. A Response Surface Methodology (RSM), based on Central Composite Design (CCD) was used for both the experimental design and the results correlation. Studied variables were pressure (from 8.0 to 15.0 MPa) and CO_2 flow rate (from 10 to 60 g·min^{-1}), while temperature (40 ^{0}C) and feed solution flow rate (0.45 mL·min^{-1}) were maintained constant. Overall achieved yields were around 70 %, being downstream vessel yields much higher than those in the precipitation vessel. The conditions predicted to reach an optimal overall yield and fractionation were 80 MPa and 10 g·min^{-1} (composite desirability = 0.7443). Casticin and artemetin were mainly obtained in the downstream vessel, being this fraction more enriched in artemetin than casticin.

Keywords

Artemisia absinthium, artemetin, casticin, Supercritical Anti-solvent Fractionation

1. Introduction

The study of natural products, that is, products obtained from both plants and animals, has witnessed a huge and unrelenting growth in the last years due to the fact that they show in many cases interesting bioactive properties (phytosanitary, antioxidant, therapeutic, etc.) and can be less noxious to health and environment than synthetic products with similar characteristics. This study covers many fields from techniques of extraction, separation and formulation to the assessment of its bioactivity.

Artemetin (A) (2-(3,4-dimethoxyphenyl)-5-hydroxy-3,6,7-trimethoxychromen-4-one) and casticin (C) (5-hydroxy-2-(3-hydroxy-4-methoxyphenyl)-3,6,7-trimethoxychromen-4-one), Fig. 1, are two flavonoids that differ by only one methyl group in position C3 of the phenyl group.

The bioactivity of both molecules has been widely studied. Artemetin has demonstrated hypotensive properties on rats [1], protective effects against contrast induced cytotoxicity by iodixanol in LLC-PK1 cells [2], antioxidant and anti-inflammatory activity [3], and anticancer action [4] among other potential therapeutic applications. Casticin has caught the attention of researchers too. The current status of casticin bioactivity as anticancer (lung, breast, cervical, pancreatic, colon, ovarian, etc) and anti-inflammatory compound has been extensively described by E. W. E. Chang et *al*. [5].

The fact that they share a high structural similarity does not mean that they would always show an analogous bioactivity. Perhaps the most clarifying example can be found in the study carried out by Elford *et al*. [6], where their efficacy against malaria was analysed; while casticin displayed better synergism than artemetin with artemisinin versus *Plasmodium falciparum*, neither would synergize with chloroquine. This fact clearly suggested a different mode of action of the compounds [6]. This different behaviour was also observed when tested on tumour cells. Thus, casticin was very effective against three human tumour cell lines (HeLa, MCF-7 and A431, being its

IC_{50} ≈1.286 μM), while artemetin was not [7]. A similar study was performed by M. Y. Huang et *al.* [8] and, once again, casticin demonstrated an elevated cytotoxicity against the PANC-1, K562, and BxPC-3 cancer cell lines, whereas artemetin was inactive. Kobayakawa et *al*. [9] also verified dissimilar results between casticin and artemetin for the inhibition of human squamous carcinoma KB cell proliferation, being casticin 70 times more powerful than artemetin.

Referring to their vegetal sources these two flavonoids have been found to occur simultaneously in several plant species, such as *Artemisia annua* [10] and *Vitex agnus-castus* [11-12,13]. Apart from that, artemetin can also be found in *Achillea millefolium* [14], *Cordia curassavica* [15], *Artemisia gorgonum* [16] and *Ageratum houstonianum* [17]; while casticin has been mainly extracted from *Vitex rotundifolia* [18], *Fructus viticis* [19] or *Croton betulaster* [20].

The first time artemetin and casticin were reported to coexist in *Artemisia absinthium* L (wormwood) extracts was in 2012 by González-Coloma et *al*. [21]. They extracted these two compounds from *A. absinthium* grown under controlled conditions in Spain. The reported yields for artemetin and casticin fractions were respectively $21.2 \cdot 10^{-3}$ % and $13.0 \cdot 10^{-3}$ % [12].

In most of the previous works focused on obtaining *A. absinthium* extracts and/or their fractions, researchers have mainly applied traditional techniques such as hydrodistillation [22], organic solvent extraction [12], aqueous extraction [23] or vapour pressure extraction (VPE) [24]. But, if *A. absinthium* extracts or their components would have a therapeutic destination, their quality and purity are points that should be taken into account. The use of high temperatures not only for extraction but also for fractionation, as in hydrodistillation or VPE, could lead to the degradation of extract

compounds, and the use of organic solvents for these two purposes might lead to the presence of solvent traces in the final product. Then, the technique employed can become a crucial issue.

Supercritical CO_2 ($scCO_2$) can be a safer option [25] to avoid these shortcomings because the temperatures involved are not high (35 – 60 ºC), CO_2 is nontoxic and the obtained extract is completely solvent-free. In fact, supercritical fluid extraction with CO_2 as solvent has been successfully applied to *A. absinthium* [22,26].

But extraction is not the only possibility of a green technology based on the use of $scCO_2$. Supercritical Anti-solvent Fractionation (SAF) or Supercritical Anti-solvent Extraction (SAE) methodologies [25,27] could become an alternative procedure for the fractionation of natural extracts and/or their enrichment (with respect their proportion in the original extract) in certain compounds, which are non-soluble in $scCO_2$.
Generally speaking, the SAF process consists of the continuous contact between $scCO_2$ and a liquid solution, usually in an organic solvent, of the plant extract in a pressurized vessel, commonly named precipitation vessel, that ensures supercritical conditions for the mixture of CO_2 and the organic solvent. A spray of this liquid solution, called feed solution, is then produced in the supercritical medium to enhance the mixing of the two fluids. Those compounds from the feed solution that are not soluble in this supercritical environment will precipitate in the precipitation vessel, while the still soluble compounds will be transported together with the $scCO_2$ and the organic solvent to a so-called downstream vessel, where they will be recovered as a liquid solution by decompression. Thus the fractionation will have taken place [25].

As far as we know, SAF has not been applied to wormwood extracts. However, this technique has been used for the selective fractionation of extracts of seed from winery residues [25], *Persea indica* [27], *Arrabidaea chica* Verlot [28], olive leaves [29], green

propolis [30], among others. But the use of SAF goes beyond because it was utilized for the optical resolution of ibuprofen enantiomers [31].

The aim of the current work was to evaluate the SAF ability both to fractionate the *A. absinthium* extracts and to enrich the fractions in the therapeutically interesting compounds, artemetin and casticin. A set of experiments (runs), in which CO_2 pressure and flow rate were varied, were designed through a Response Surface Methodology (RSM), based on Central Composite Design (CCD) that was also used to correlate the results. Yields (w/w %) for every fraction were determined and artemetin and casticin were quantified in the feed solution and in every fraction.

2. Materials and methods

2.1. Raw material preparation and characterization

A. absinthium plants were grown under controlled conditions in Ejea de los Caballeros, northeast of Spain. They were collected in 2017. Dried wormwood leaves and flowers had a 9.36 % ± 0.37 humidity content, measured with a Sartorius model MA 40 Moisture Analyzer Software/ hardware 01.05.02. Moisture content was measured using 0.5 g of plant and repeated five times.

Plant material (wormwood dried leaves and flowers) was ground using an electric grinder. A vibratory sieve shaker CISA model BA 300N was used to analyze the particle size distribution. The average diameter of particles, d_{mg}, was 0.419 mm. It was calculated according to ANSI/ASAE S319.3 from the American National Standards Institute [32].

2.2. Feed Solution preparation

150 g of *A. absinthium* flowers and leaves were first macerated in hexane for 48 h (defatting) and then in ethanol for the same time to extract the more polar compounds. The final solvent-free extract was dissolved in ethanol at an approximate concentration of 3% (w/w) and filtered (Minisart NML cellulose acetate 0.2 μm) later to get the feed solution (FS) used for the fractionation experiments. This organic solvent was chosen because it guaranteed the dissolution of the compounds of interest and it is considered as a non-toxic and eco-friendly.

2.3. Supercritical Anti-solvent Fractionation

A lab-scale apparatus, Fig.2, was used to carry out the SAF experiments. Its main components are a CO_2 pump (P-SCF), an extract solution pump (P-LIQ), a 0.5 L precipitation vessel (PV) and a 0.5 L downstream vessel (DV). The working limits of the whole device are 40.0 MPa and 90 ºC. Pressure, flow rate and temperature can be automatically controlled [25].

In this work, PV temperature was 40 ºC and pressure range from 8.0 to 15.0 MPa, while DV working conditions (3.0 MPa, 25 ºC) were closer to room conditions not to lose compounds of interest. CO_2 flow rate varied from 10 to 60 $g \cdot min^{-1}$ and feed solution flow rate remained constant at 0.45 $mL \cdot min^{-1}$ for all the experiments according to previous researches [25,27].

A typical run starts by the stabilization of pressure, temperature and CO_2 flow rate in the system (PV and DV) followed by a stabilization of liquid flow by injecting liquid solvent (≈90 min, nozzle Ø =100 μm). Once the whole system is stabilized, 30 mL of feed solution is pumped into PV for almost 1 h. Using the same flow conditions, 30 mL more of pure ethanol are then pumped to wash the remaining feed solution from the pipes. Finally, only CO_2 flow is maintained for about 30 min to wash out the residual

solvent. The solid in PV, when obtained, was re-dissolved with ethanol after taking a sample for electron microscopy. All of these samples (PV and DV) were dried using a Büchi R-200 equipped with a heat bath B-490 and a controllable vacuum pump V-800. The working temperature and pressure to completely dry the samples were specified by the device taking into account the vapour pressure of the solvent to eliminate, the bath temperature where the evaporating flask is placed and the refrigeration temperature of the condenser. For ethanol, the working pressure was 67-70 mbar and the working temperature 42 ºC. The samples were kept at -20 ºC until their analysis.

Yields for PV and DV collected fractions, Y_{PV} (wt%) and Y_{DV} (wt%), respectively, were calculated using Eq. (2):

$$Y_i\ (wt\%) = 100 \times (Mass\ of\ collected\ fraction\ in\ i\ /\ Mass\ of\ extract\ in\ FS) \quad \text{Eq. (2)}$$

where *i* is the vessel where the fraction was collected, that is, PV or DV.

The *overall yield of the SAF process*, Y_{SAF} (wt%), was defined according to Eq. (3).

$$Y_{SAF}\ (wt\%) = Y_{PV}\ (wt\%) + Y_{DV}\ (wt\%) \quad \text{Eq. (3)}$$

2.4. Chromatographic tracking of Artemetin and Casticin

The tracking of artemetin and casticin was carried out with a HPLC-PDA on a HPLC *Waters® Alliance 2695* with a *PDA Waters® 2998* detector. A *CORTECS®* C18 2.7 µm (4.6x150 mm) was used together with a pre-column CORTECS® Pre-column VanGuard C18 2.7 µm (2.1x5 mm). The samples were eluted with a mobile phase acetic acid:Milli-Q water: acetonitrile (30:60:10) for 10 min, then 30:10:60 for 8 min and finally 30:60:10 for 7 min. The used flow rate was 0.8 mL/min and the temperature of 40 ºC. The detection wavelength was fixed at 340 nm. Extract solutions (100 ppm approximately) were filtered before every analysis through a *GH Polypropylene*

membrane ACRODISC 13 mm 0.2 μm Ø filter. Artemetin and casticin standards, obtained as shown in their previous work [21], were kindly provided by Dr. González-Coloma. Standards were run under the same chromatographic conditions as fractionated samples. The analyses were performed in triplicate.

Values for *single compound proportions*, $C_{i/j}$, in each sample (FS, PV and DV) were calculated as follows:

$$C_{i/j} = \frac{mass\ of\ compound\ i\ in\ fraction\ j}{mass\ of\ \text{fraction j}} \quad \text{Eq. (4)}$$

where *i/j* means that compound *i* (A for artemetin or C for casticin) has been collected in sample *j* (FS, PV or DV).

Once the $C_{i/j}$ was obtained, the *Enrichment ratio*, $E_{i/j}$, for every compound was calculated in PV and DV according to Eq. (5):

$$E_{i/j} = \frac{C_{i/j}}{C_{i/FS}} \quad \text{Eq. (5)}$$

where *i* is the specific compound (A or C), *j* is the vessel where the fraction was collected, $C_{i/j}$ is the single compound proportion in fraction *j* (PV or DV) and $C_{i/FS}$ is the single compound proportion for compound *i* in fraction FS. When $E_{i/j}$ is higher than 1, we will assume that the fraction has been enriched in compound *i* with respect to the FS.

With $E_{i/j}$ values, we finally obtained the *Relative Enrichment ratio*, RE_j, in PV and DV calculated as follows:

$$RE_j = \frac{E_{A/j}}{E_{C/j}} \quad \text{Eq. (6)}$$

where *j* is the PV or DV, $E_{A/j}$ and $E_{C/j}$ are the *Enrichment ratio* for artemetin and casticin in vessel *j* respectively. If RE_j is higher than 1, we will assume the fraction *j* is more

enriched in artemetin and less in casticin. If RE_j is lower than 1, the opposite will be assumed.

2.5. Microscopy observations

The solid morphology of the precipitated fraction obtained in PV by SAF was analysed by scanning electron microscopy (SEM) at the Electron Microscopy service, from Zaragoza University (Spain). A LEO 420 version V2.04, from Assing was used. Extracted solids were placed on a carbon tab previously stuck to an aluminium stub (Agar Scientific, Stansted, UK). Samples were coated with gold-palladium using a sputter coater (mod. 108A, Agar Scientific).

2.6. Experimental design and data analysis

To evaluate the influence of pressure and CO_2 flow rate in a statistically reliable way, a Response Surface Methodology (RSM), based on Central Composite Design (CCD), was employed. Pressure and CO_2 flow rate were respectively coded as X_1 and X_2. Feed solution concentration and flow rate, as well as temperature in PV, were set as fixed.

This same methodology allows correlating the dependence of the *Yields* and *Relative Enrichment ratio* on the variables through the following equation.

$$Y = \beta_0 + \sum_{i=1}^{2} \beta_{ii} X_i + \sum_{i=1}^{2} \beta_{ii} X_i^2 + \sum_{i \neq j=1}^{2} \beta_{ij} X_i X_j \qquad \text{Eq. (7)}$$

where Y is the dependent variable; β_0, β_{ii} and β_{ij} are fitting coefficients, and X_i and X_j are independent variables which influence is under study, that is, pressure and CO_2 flow rate.

The software *Minitab® 17* was used to carry out the RSM design based on CCD. This design for 2 variables established 13 random runs, being the centre repeated 5 times according to the range levels of the cited variables. *Minitab® 17* was also used to

determine the values of coefficients β in Eq. (7) as well as their significance ($p < 0.05$) and the optimal conditions for the maximum *overall yield of the SAF process*. The range and levels of independent factors, pressure (P) and CO_2 flow rate (Q), is given in Table 1.

2.7. Chemicals and reagents

The solvents used in the extraction process were hexane (Panreac 99.0%), ethanol (AnalaR Normapure 99.96%) and CO_2 (Alpha Gas 99.8%). HPLC-PDA mobile phase solvents were water (MilliQ 18.2 MΩ·cm), acetic acid (Sigma-Aldrich 99.5%) and acetonitrile (Scharlab 99.9%).

3. Results and discussion

3.1. Experimental design

For the application of the RSM design based on CCD, values for pressure, X_1, were set between 8.0 and 15.0 MPa (axial points), whereas for CO_2 flow rate, X_2, were set between 10 and 60 $g \cdot min^{-1}$ (axial points). These values were chosen because they led to good results according to previous experiments [25, 27]. For the central experiment, X_1 and X_2 were 11.5 MPa and 35 $g \cdot min^{-1}$, respectively. Data for all of the runs are gathered in Table 2, where the experimental order of the experiments, given by the experimental design, is offered on the second column, *Exp. Run. Ord*er. Values of FS concentration, FS flow rate and temperature in PV were 3% (w/w), 0.45 $mL \cdot min^{-1}$ and 40 ^{o}C, respectively. These working conditions provided a CO_2 molar fraction close to 0.98 for all of the runs, which ensures that supercritical conditions are attained for the mixture (CO_2 + ethanol) [25].

3.2. Yields

First of all, it must be said that a powder was precipitated in PV only in Runs 3, 5-9 and 11. As an example, Fig. 3 shows two SEM images of the powder collected in experiments 6 and 8, which morphology and size are representative of the other powders. It can be appreciated that the particles are aggregates of smaller particles (1-10 μm approximately) that have a spherical shape.

Experimental values for Y_{PV} (wt%), Y_{DV} (wt%) and Y_{SAF} (wt%) for every run are also listed in Table 2. Y_{PV} (wt%) oscillates between 7.4 (run 4) and 29.9 % (run 5), Y_{DV} (%) changes between 32.9 (run 13) and 58.3 % (run 2). It can be seen that yields in DV generally are generally twice as high as the yields in PV, but greater ratios are observed for runs 2 and 4 where Y_{DV} (wt%) are 5.6 and 7.9 times Y_{PV} (wt%), respectively.

Only Y_{PV}, Y_{DV}, $E_{C/PV}$ and RE_{DV} were successfully fitted using Eq. 7. In Table 3, the fitting coefficients of this equation are gathered for the cited parameters as a function of pressure, X_1 (MPa), and CO_2 flow rate, X_2 ($g \cdot min^{-1}$). In Figs. 4 and 5, the contour plots corresponding to the surfaces defined by Eq. (7) are given for these yields. Y_{DV} (wt%) depends on all the terms but Y_{PV} (wt%) does not depend on the cross term $X_1 \cdot X_2$. Although not all the coefficients are statistically significant, the regression coefficients are high for both yields, this means that a reliable analysis of the influence of pressure and CO_2 flow rate can be carried out from Figs. 4 and 5.

Then, in Fig. 4, it can be seen that Y_{PV} (wt%) shows a zone of maximum values at CO_2 flow rates between 17 and 35 $g \cdot min^{-1}$ and pressures between 8.5 and 12.0 MPa. Within these ranges of pressure and CO_2 flow rate, Y_{PV} (wt%) initially increases as the pressure increases at a given CO_2 flow rate, then significantly diminishes when the pressure is further increased. The same could be said if the CO_2 flow rate is increased at a given pressure: an initial increase in Y_{PV} (wt%) is followed by a decrease which, in this case,

is less pronounced. Out of the ranges of pressure and CO_2 flow rate limiting the zone of the maximum yield, a decrease of Y_{PV} (wt%) is observed when either the pressure is increased at a given CO_2 flow rate or the CO_2 flow rate is increased at a given pressure. In any case, the lowest yields in PV are reached at high values of CO_2 flow rate, especially at high pressure, which is consistent, for example, with run 2 from Table 2 (10.5 % at 14.0 MPa and 53 $g \cdot min^{-1}$).

On the other hand, according to Fig. 5, Y_{DV} (wt%) increases with pressure for every studied CO_2 flow rate whenever this pressure is above 14.0 MPa. This effect becomes more marked at higher flow rates. If the pressure is below this value, Y_{DV} (wt%) first decreases with increasing CO_2 flow rates and then Y_{DV} (wt%) becomes higher. The highest Y_{DV} (wt%) is found for high pressure and high CO_2 flow rate and it is possible that greater Y_{DV} (wt%) could be found with further increase of the variables.

3.3. Enrichment ratios

Parallel to the performance of SAF experiments, the track of artemetin and casticin was carried out for the FS and for every fraction precipitated in both PV and DV. As mentioned above, artemetin and casticin are both flavonoids which differ in the presence of an ether group, instead of an alcohol one, in artemetin, turning this molecule into a less polar one. This is consistent with the fact that artemetin is eluted before casticin when the chromatographic analysis was carried out, Fig 6.

Enrichment parameters, such as $E_{i/j}$ and RE_j are listed in Table 2. Neither $E_{A/PV}$ nor RE_{PV} are included because the amount of artemetin in PV was under the chromatographic detection limit. Artemetin and casticin proportions in the FS, $C_{A/FS}$ and $C_{C/FS}$, respectively, were 0.02 for both of them, which means a RE_{FS} of 1.00. By and large, $E_{C/PV}$ values are significantly lower than $E_{C/DV}$ and $E_{A/DV}$, indicating that these two

compounds are more concentrated in DV than in PV. The only exception occurs for run 13 where $E_{C/PV}$ is slightly greater than $E_{C/DV.}$ Observing $E_{C/PV}$ values, we could state that, according to data from Table 2, casticin solubility in $scCO_2$ decreases with pressure.

Fitting coefficients of Eq. 7 for $E_{C/PV}$ and for RE_{DV} as a function of pressure, X_1 (MPa), and CO_2 flow rate, X_2 ($g \cdot min^{-1}$) are given in Table 3. The other parameters didn´t fit this equation.

According to Table 3, the fact that β_{22} and β_{12} don´t take part in the equation means that the dependence of $E_{C/PV}$ with pressure is stronger than with CO_2 flow rate, reaching the highest $E_{C/PV}$ values for the lowest pressure (see runs 11 to 13 from Table 2). For a given pressure, $E_{C/PV}$ increases when the CO_2 flow rate diminishes, Fig. 7 and Table 2. This behaviour can be observed in runs 4, 5 to 9 and 10. In all these experiments, pressure was 11.5 MPa and flow rate changes from 60 to 10 $g \cdot min^{-1}$, while the $E_{C/PV}$ increases from 0.03 (run 4) to 0.15 (run 10).

In Fig. 8, the contour plot corresponding to the surface defined by Eq. 7 can be found. RE_{DV} does not depend on the quadratic term for the CO_2 flow rate (X_2^2) nor on the cross term $X_1 \cdot X_2$. All the coefficients are statistically significant, excepting that of the CO_2 flow rate (X_2). Accordingly, the regression coefficient is very high. Then, the analysis of the influence of pressure and CO_2 flow rate can be carried out very reliably from Fig. 8. RE_{DV} increases as the pressure becomes lower at any given CO_2 flow rate if pressure is below 13.0 MPa. At higher values of pressure, an increase in RE_{DV} is observed when pressure increases too. However, at a given working pressure there is no significant variation in RE_{DV} with CO_2 flow rate except in the range 12-14 MPa where a slight decrease is seen. It must be said that the experimental results at 9.0 MPa (runs 11 and

12) do not coincide with the contour plot because the experimental value of RE_{DV} in run 11 is 1.26 and, according to the contour plot it should be placed between 1.4 and 1.6.

Although the research by González-Coloma et *al*. revolves around *Persea indica* [27] and this is a different plant from *A. absinthium*, it can be observed that the tracked molecule in their SAF process, ryanodol, was also more concentrated in DV than in PV, as it happened in this work with casticin and artemetin, (values of $E_{i/DV}$ higher than 1.00 and values of $E_{i/PV}$ lower than 1.00, Table 2). However, and regarding RE_{DV} values, the fact that they are higher than 1.00 for all the experiments concludes that artemetin precipitated in a higher proportion than casticin in DV, which is consistent with the fact that artemetin is less polar and/or with lower dielectric constant than casticin, that is why on the one hand artemetin is eluted first in the chromatogram and, on the other hand, we find a certain amount of casticin in PV but chromatographically undetectable amounts of artemetin.

Then, the difference in their chemical structure seems to be enough to get an enriched fraction of *A. absinthium* extracts in artemetin. Within the cautions due to experimental inaccuracies, the applied RSM model provides us the upper limit of working conditions to achieve a significant enrichment of the compounds of interest. Values of RE_{DV} = 1.60 and $E_{C/PV}$ = 0.5 together with a recovering 65 % of the feed solution (Y_{PV} = 20%, Y_{DV} = 45%) can be obtained operating up to 87 bar and CO_2 flow rate of 17 $g \cdot min^{-1}$.

4. Conclusions

In this work, the SAF methodology was applied to conventional extracts from *Artemisia absinthium* (wormwood) to evaluate its ability to fractionate those extracts and through the tracking of two therapeutically interesting compounds with high structural similarity, artemetin and casticin, its ability to enrich the fractions in those compounds.

To achieve this goal, we used a Response Surface Methodology (RSM), based on Central Composite Design (CCD), to design the set of experiments and to carry out the correlation of some of the results with the variables selected for the SAF process. These variables were pressure (varying from 8.0 to 15.0 MPa) and CO_2 flow rate (varying from 10 to 60 $g \cdot min^{-1}$), while temperature (40 ºC) and feed solution flow rate (0.45 $mL \cdot min^{-1}$) were kept constant.

Obtained overall yields were around 70 %, being downstream vessel yields much higher than those in the precipitation vessel. Casticin and artemetin were mostly obtained in the downstream vessel, being this fraction enriched in both compounds when compared to their proportion in the feed solution. Besides, downstream vessel fraction was found to have a higher ratio of artemetin than casticin; so despite their minor difference in chemical structure, and, in fact, likely due to it, SAF seems to be able to get an enriched fraction of *Artemisia absinthium* extracts in one of these compounds, artemetin. Optimal pressure and flow rate values are found towards the lower limits of the ranges considered for these properties. Taken into account the limitation imposed by the experimental uncertainty, the predicted conditions to reach an optimal overall yield and fractionation were about 8.0 MPa and 10 $g \cdot min^{-1}$ (composite desirability = 0.7443).

Acknowledgement

The authors are grateful for the financial support of MINECO-FEDER (Project CTQ2015-64049-C3-2-R) and of Departamento de Innovación, Investigación y Universidad del Gobierno de Aragón-FEDER-FSE "Construyendo Europa desde Aragón" (Grupo E39_17R).

We also would like to thank J. Burillo from CITA (Centro de Investigación Agroalimentario de Aragón), Spain, for having supplied the plant material.

Table 1. Range and levels of independent factors: pressure (P) and CO_2 flow rate (Q)

Factors	Symbol	Range and levels of independent factors				
		-1.41	-1	0	1	1.41
P_{CO_2} (MPa)	(X_1)	8.0	9.0	11.5	14.0	15.0
Q_{CO_2} ($g \cdot min^{-1}$)	(X_2)	10	17	35	53	60

Where X_1 corresponds to Pressure and X_2 to CO_2 flow rate; T = 40 ºC; Q_{FS} = 0.45 $mL \cdot min^{-1}$

Table 2. Working conditions (X_1/MPa and X_2/g·min^{-1}); PV, DV and SAF yields (Y_{PV}, Y_{DV} and Y_{SAF}/ %, respectively); PV enrichment ratio for C ($E_{C/PV}$); DV enrichment ratio for C and A ($E_{C/DV}$ and $E_{A/DV}$ respectively); DV relative enrichment ratio (RE_{DV}). First column on the left, *Run*, shows the numbering the experiments are referred to in the text. Second column on the left, *Exp. Run. Ord*er, shows the experimental order, given by the experimental design, the runs were carried out.

							PV	**DV**		
Run	**Exp. Run Order**	X_1/ **MPa**	X_2/ **g·min^{-1}**	Y_{PV}/ **wt%**	Y_{DV}/ **wt%**	Y_{SAF}/ **wt%**	$E_{C/PV}$	$E_{C/DV}$	$E_{A/DV}$	RE_{DV}
1	1	15.0	35	16.3	52.5	68.8	0.03	1.00	1.02	1.02
2	4	14.0	53	10.5	58.3	68.8	0.02	0.96	0.96	1.00
3	2		17	23.6	53.1	76.7	0.07	1.29	1.36	1.05
4	3	11.5	60	7.4	58.2	65.6	0.03	1.17	1.18	1.01
5	7		35	29.9	44.7	74.6	0.06	1.42	1.51	1.07
6	8			24.0	44.8	68.8	0.05	1.33	1.43	1.07
7	9			24.2	42.0	66.2	0.05	0.93	0.95	1.02
8	13			22.7	50.0	72.7	0.12	1.08	1.18	1.09
9	11			21.1	48.9	70.0	0.02	1.55	1.59	1.03
10	6		10	18.4	50.4	68.8	0.15	0.94	1.00	1.07
11	5	9.0	53	17.3	41.0	58.3	0.21	1.10	1.38	1.26
12	10		17	28.3	48.4	76.7	0.38	0.98	1.39	1.41
13	12	8.0	35	19.3	32.9	52.2	0.68	0.65	1.24	1.89

Where X_1 corresponds to Pressure and X_2 to CO_2 flow rate; T = 40 ºC; Q_{FS} = 0.45 mL·min^{-1}

Table 3. Fitting coefficients of Eq. 7 for PV and DV yields (Y_{PV}, Y_{DV}/% respectively), casticin enrichment ratio in PV ($E_{C/PV}$) and DV relative enrichment ratio (RE_{DV}) along with the corresponding regression coefficients, R, and standard deviation, s.

	Y_{PV}/ %		Y_{DV}/ %		$E_{C/PV}$		RE_{DV}	
	Coefficient value	p	Coefficient value	p	Coefficient value	p	Coefficient value	p
β_0	-20.9	0.000	34.2	0.000	3.868	0.000	6.216	0.000
β_1	0.724	0.160	0.476	0.001	-0.05733	0.000	0.0795	0.000
β_2	0.751	0.005	-1.775	0.366	-0.00274	0.059	0.00194	0.292
β_{11}	-0.00349	0.157	-0.00207	0.339	0.000218	0.000	0.000305	0.000
β_{22}	-0.01474	0.010	0.01443	0.008	-		-	-
β_{12}	-	-	0.00720	0.095	-		-	-
R^2	0.7897		0.8753		0.9164		0.9098	
s	3.6		3.3		0.06		0.09	

Where subscript 1 corresponds to Pressure and subscript 2 to CO_2 flow rate

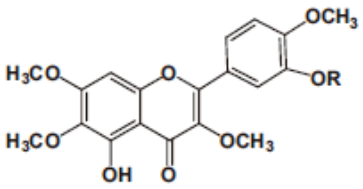

I **R = OCH_3**

II **R = OH**

Fig. 1. Chemical structures for artemetin (I) and casticin (II).

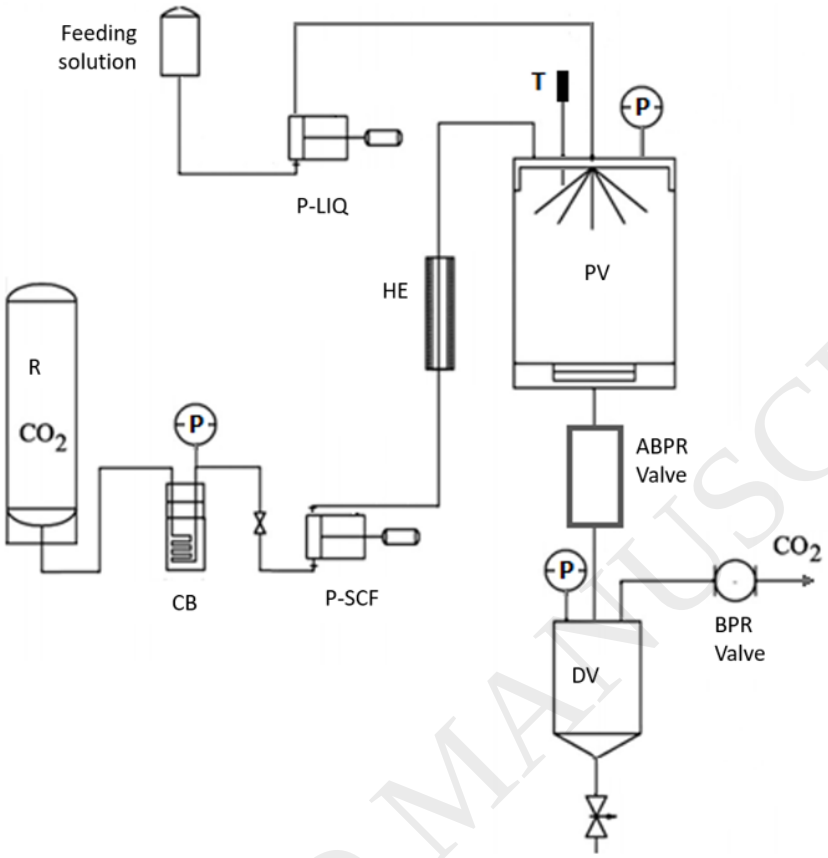

Fig. 2. Scheme of the SAF plant. CO_2 pump (P-SCF); liquid (extract) pump (P-LIQ); CO_2 reservoir (R); precipitation vessel (PV); cooling bath (CB); heat exchanger (HE); automated back pressure regulator (ABPR); back pressure regulator (BPR); downstream vessel (DV).

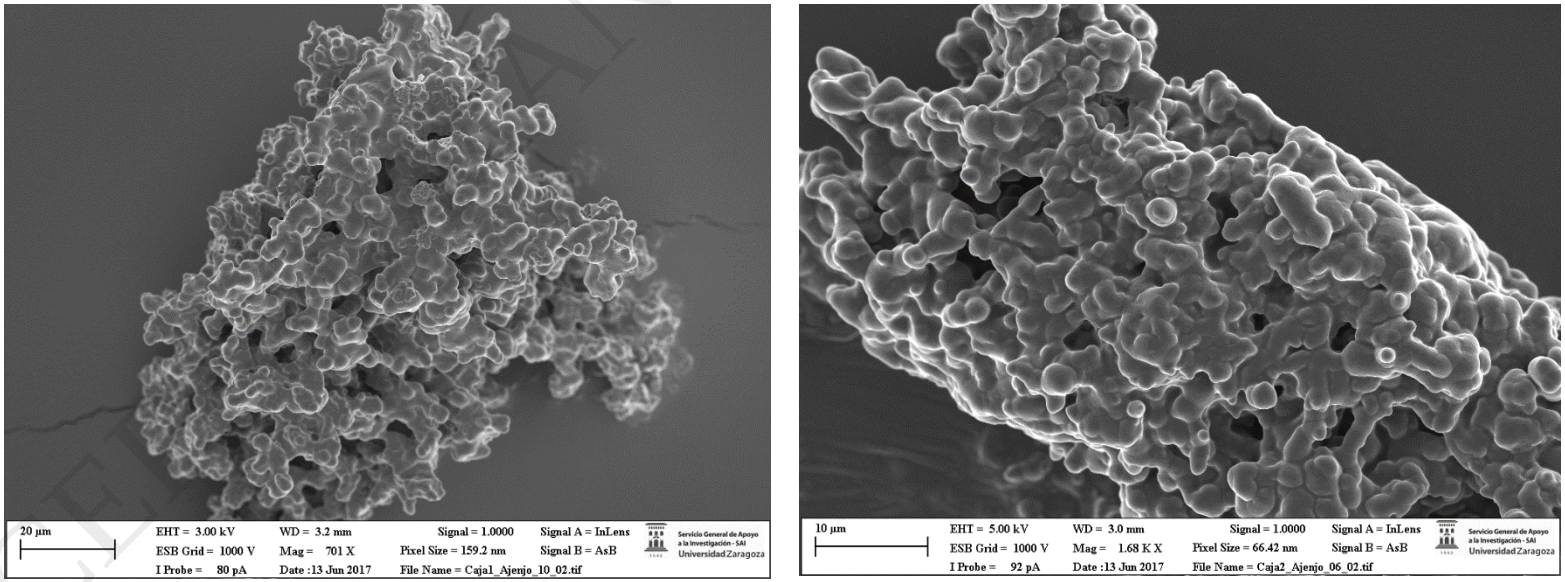

Fig. 3. SEM images of powder samples collected in PV for experiments 6 (left) and 8 (right).

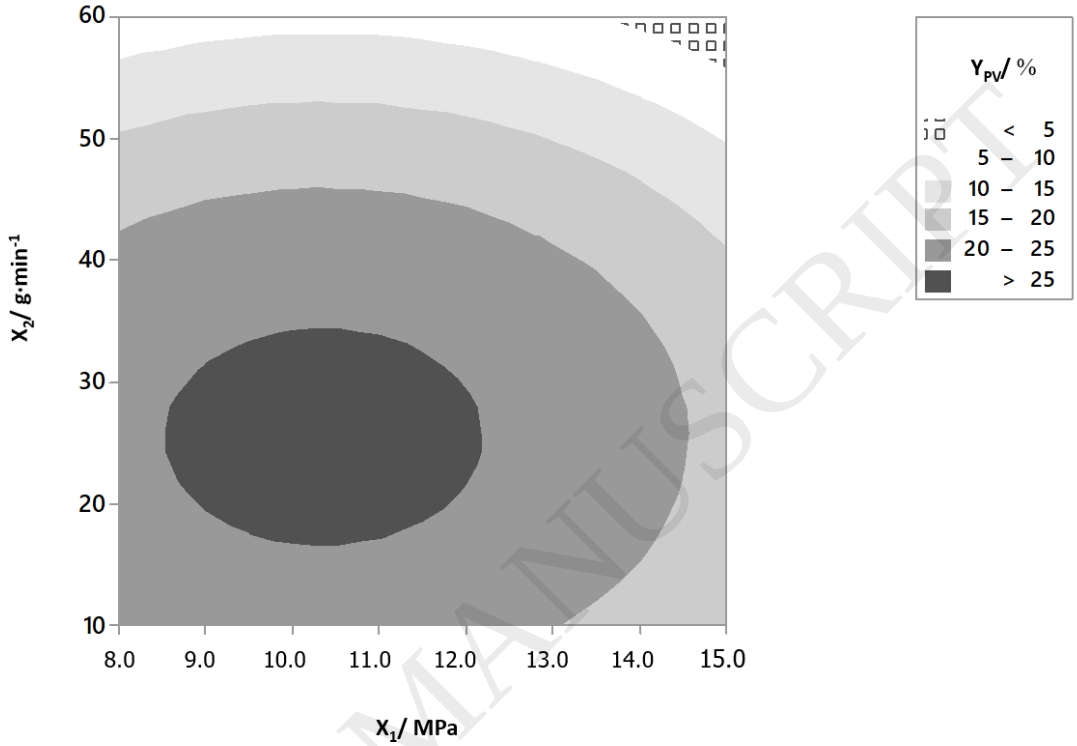

Fig. 4. Contour plot of Y_{PV}/ % versus X_1 (Pressure/MPa) and X_2 (CO_2 flow rate/g·min^{-1})

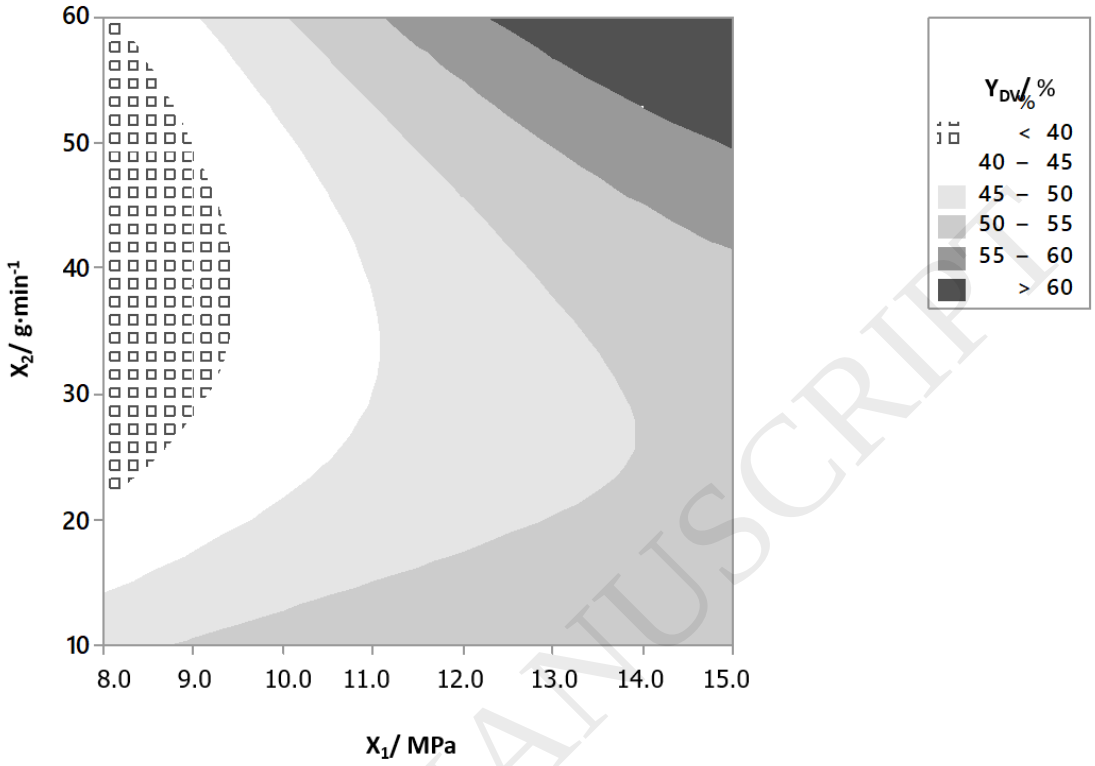

Fig. 5. Contour plot of Y_{DV}/ % versus X_1 (Pressure/MPa) and X_2 (CO_2 flow rate/g·min^{-1}).

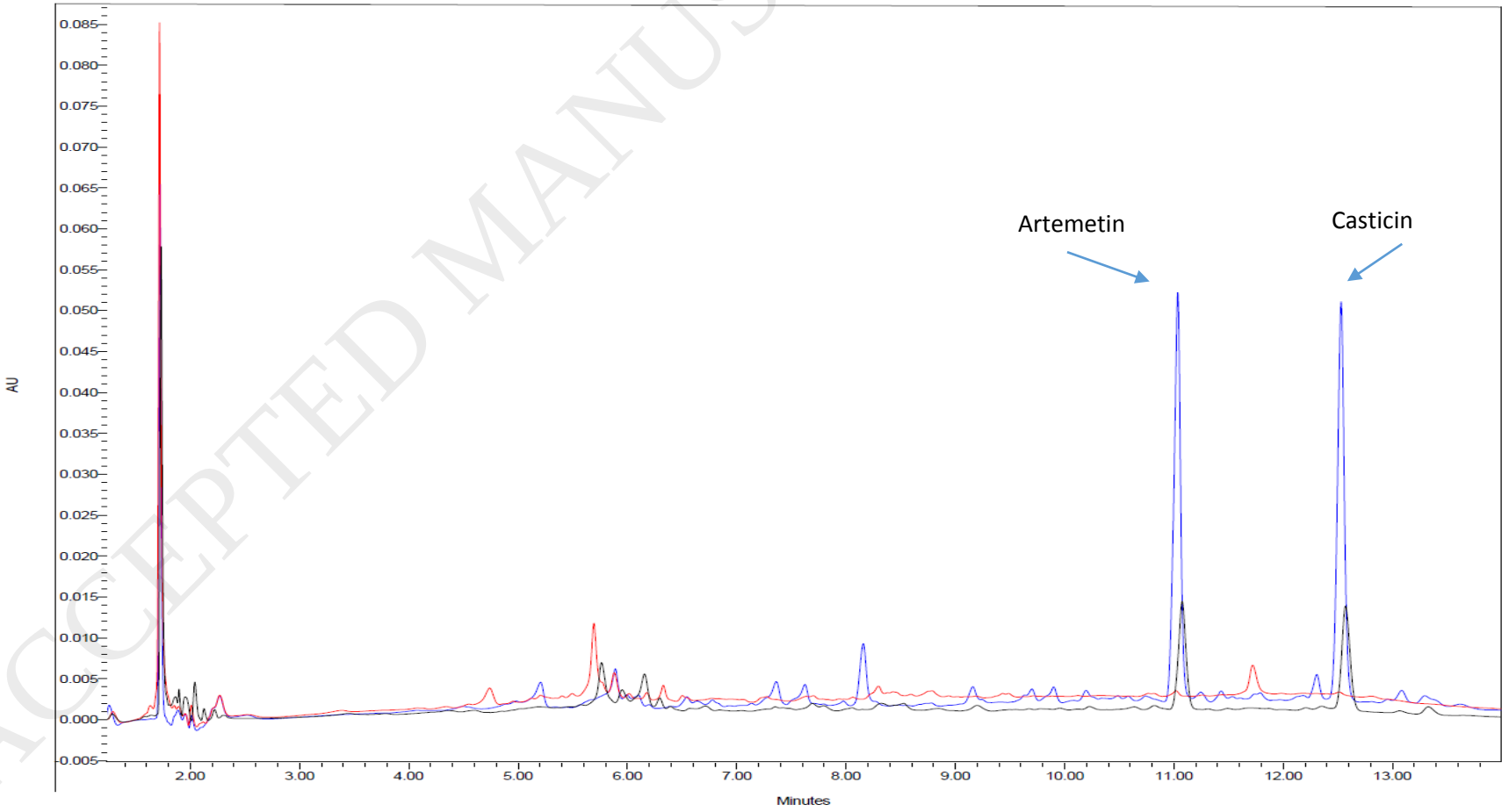

Fig. 6. Chromatogram of experiment 9. Artemetin at retention time = 11.12 min. Casticin at retention time = 12.57 min. PV fraction, line red. DV, line blue, FS line black.

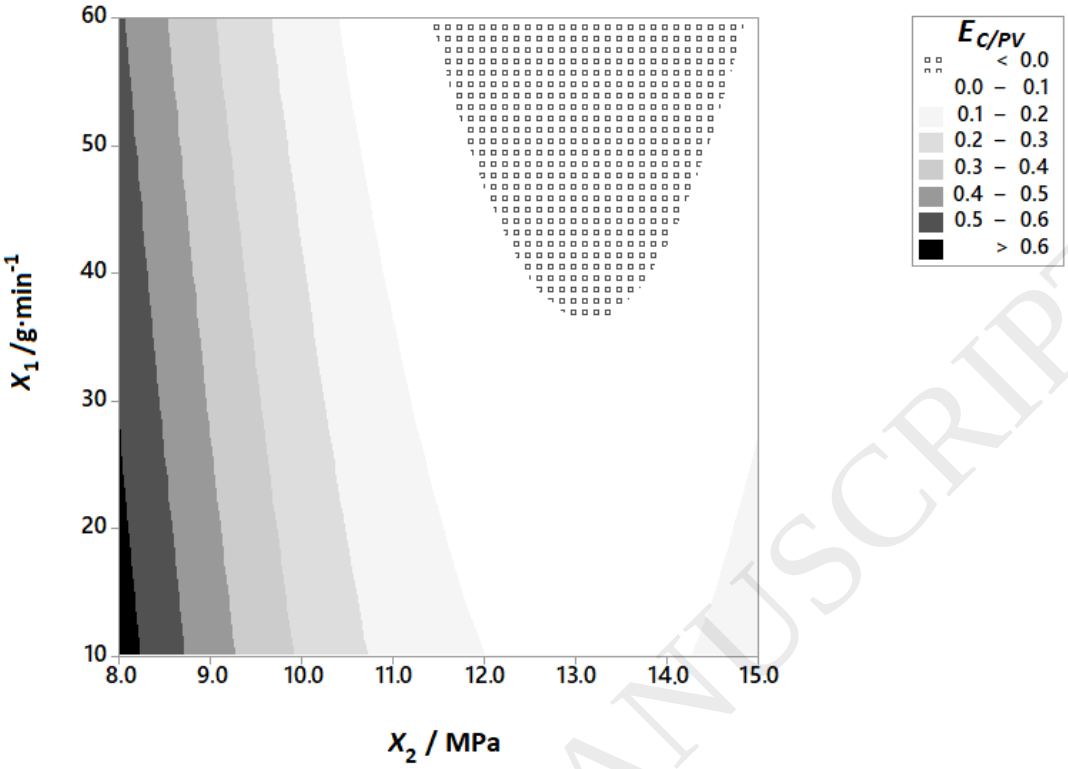

Fig. 7. Contour plot of $E_{C/PV}$ versus X_1 (Pressure/MPa) and X_2 (CO_2 flow rate/g·min^{-1}).

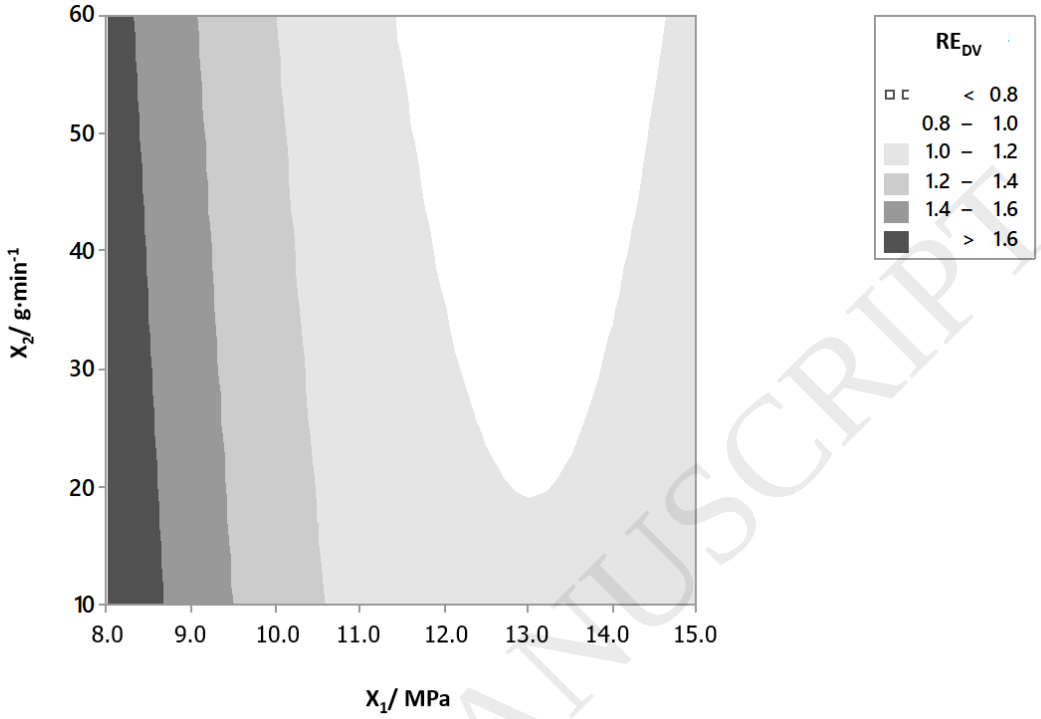

Fig. 8. Contour plot of RE_{DV} versus X_1 (Pressure/MPa) and X_2 (CO_2 flow rate/g·min^{-1}).

References

[1] P. de Souza, A. Gasparotto Jr., S. Crestani, M. É. A. Stefanello, M. C. A. Marques, J. E. da Silva-Santos, C, A. L. Kassuya, Hypotensive mechanism of the extracts and artemetin isolated from *Achillea millefolium* L. (Asteraceae) in rats, Phytomed 18 (2011) 819-825

[2] D. Lee, C. E. Kim, S. Y. Park, K. O. Kim, N. T. Hiep, D. Lee, H. J. Jang, J. W. Lee, K. S. Kang, Protective effect of *Artemisia argyi* and its flavonoid constituents against contrast-induced cytotoxicity by iodixanol in LLC-PK1 cells, Int. J. Mol. Sci. 19(5) (2018) 1387

[3] J. Hu, W. Ma, N. Li, K. J. Wang, Antioxidant and Anti-Inflammatory Flavonoids from the Flowers of Chuju, a Medical Cultivar of *Chrysanthemum morifolim* Ramat, J. Mex. Chem. Soc. 61(4) (2017) 282-289

[4] W. X. Li, C. B. Cui, B. Cai, H. Y. Wang, X. H. Yao, Flavonoids from *Vitex trifolia* L. inhibit cell cycle progression at G(2)/M phase and induce apoptosis in mammalian cancer cells, J. Asian Nat. Prod. Res. 7(4) (2005) 615-626

[5] E. W. C. Chan, S. K. Wong, H. T. Chan, Casticin from *Vitex* species: a short review on its anticancer and anti-inflammatory properties, J. Integr. Med. 16 (2018) 147-152

[6] B. C. Elford, M. F. Roberts, D. Phillipson, R. J. M. Wilson, Potentiation of the antimalarial activity of quinghaosu by methoxylated flavones. Trans. Roy. Soc. Trop. Med. 81 (1987) 434-436

[7] B. Csupor-Loffler, Z. Hajdu, I. Zupko, B. Rethy, G. Falkay, P. Forgo, J. Hohmann, Antiproliferative effect of flavonoids and sesquiterpenoids from *Achillea millefolium* s.l. on cultured human tumour cell lines Phytother. Res. 23(5) (2009) 672-676

[8] M. Y. Huang, L.J. Zhong, J. M. Xie, F. Wang, Y. H. Zhang, A new taraxastane-type triterpene from *Vitex trifolia* var. *simplicifolia*. Helv. Chim. Acta 96(11) (2013) 2040-2045

[9] J. Kobayakawa, F. Sato-Nishimori, M. Moriyasu, Y. Matsukawa, G2-M arrest and antimitotic activity mediated by casticin, a flavonoid isolated from *Viticis Fructus* (*Vitex rotundifolia* Linne fil.) Cancer Lett. 208(1) (2004) 59-64

[10] P. J. Weathers, M. J. Towler, The flavonoids casticin and artemetin are poorly extracted and are unstable in an *Artemisia annua* tea infusión, Planta Med. 78(10) (2012) 1024–1026

[11] S. Li, S. Qiu, P. Yao, H. Sun, H. H. S. Fong, H. Zhang, Compounds from the Fruits of the Popular European Medicinal Plant *Vitex agnus-castus* in Chemoprevention via NADP(H):Quinone Oxidoreductase Type 1 Induction, J. Evid. Based Complementary Altern. Med. (2013) 432829

[12] M. I. Choudhary, Azizuddin, S. Jalil, S. A. Nawaz, K. M. Khan, R. B. Tareen, Atta-ur-Rahman, Antiinflammatory and Lipoxygenase Inhibitory Compounds from *Vitex agnus-castus*, Phytother. Res. 23 (2009) 1336-1339

[13] Azizuddin, M. Iffat, M. I.Choudhary, K. M. Kahn, Antifungal, Antibacterial, Phytotoxic and Cytotoxic Potential of Casticin Isolated from *Vitex agnus-castus*, J. Chem. Soc. Pak. 34(5) (2012) 1286-1289

[14] P. de Souza, A. Gasparotto Jr., S. Crestani, M. E. Alves Stefanello, M. C. Andrade Marques, J. E. da Silva-Santos, C. A. Leite Kassuya, Hypotensive mechanism of the extracts and artemetin isolated from *Achillea millefolium* L. (Asteraceae) in rats, Phytomedicine, 18 (2011) 819-825

[15] M. C. Bayeux, A. T. Fernandes, M. A. Foglio, J. E. Carvalho, Evaluation of the antiedematogenic activity of artemetin isolated from *Cordia curassavica* DC, Braz. J. Med. Biol. Res. 35 (2002) 1229-1232

[16] A. Martins, R. Mignon, M. Bastos, D. Batista, N. R. Neng, J. M. F. Nogueira, C. Vizetto-Duarte, L. Custódio, J. Varela, A. P. Rauter, In vitro Antitumoral Activity of Compounds Isolated from *Artemisia gorgonum* Webb, Phytother. Res 28 (2014) 1329-1334

[17] I. Sánchez, J. Calderón, B. Ruiz, J. Tellez, L. Calzada, J. Taboada, *In vitro* Cytotoxicity of Flavonoids Against MK2 and C6 Tumour Cells Phytother. Res 15 (2001) 290-293

[18] C. J. Liou, W. C. Huang, Casticin inhibits interleukin-1β–induced ICAM-1 and MUC5AC expression by blocking NF-κB, PI3K-Akt, and MAPK signalling in human lung epithelial cells, Oncotarget 8(60) (2017) 101175-101188

[19] Y. Zhou, L. Tian, L. Long, M. Quan, F. Liu, J. Cao, Casticin Potentiates TRAIL-Induced Apoptosis of Gastric Cancer Cells through Endoplasmic Reticulum Stress, PLOS ONE 8(3) (2013) 1-11

[20] T. C. Leite de Sampaio e Spohr, J. Stipursky, A. Campos Sasaki, P. Rocha Barbosa, V. Martins, C. Farias Benjamim, N. Franca Roque, S. Lima Costa, F. Carvalho Alcantara Gomes, Effects of the Flavonoid Casticin From Brazilian *Croton betulaster* in Cerebral Cortical Progenitors In Vitro: Direct and Indirect Action Through Astrocytes, J. Neurosci. 88 (2010) 530-541

[21] A. González-Coloma, M. Bailén, C. E. Díaz, B. M. Fraga, R. Martínez-Díaz, G. E. Zuniga, R. A. Contreras, R. Cabrera, J. Burillo, Major components of Spanish cultivated *Artemisia absinthium* populations: Antifeedant, antiparasitic, and antioxidant effects, Ind. Crops Prod. 37 (2012) 401-407

[22] L. Martín, A. González-Coloma, J. Burillo, A. M. F. Palavra, J. S. Urieta, A. M. Mainar, Microcalorimetric determination of the activity of supercritical extracts of wormwood (*Artemisia absinthium* L.) over *Spodoptera littoralis,* J. Therm. Anal Calorim. 11(3) (2013) 1837-1844

[23] M. Ali, B. Kim, K. D. Belfield, D. Norman, M. Brennana, G. S. Ali, Green synthesis and characterization of silver nanoparticles using *Artemisia absinthium* aqueous extract — A comprehensive study, Mater. Sci. Eng. C. 58 (2016) 359-365

[24] L. F. Julio, A. González-Coloma, J. Burillo, C. E. Díaz, M. F. Andrés, Nematicidal activity of the hydrolate byproduct from the semi-industrial vapour pressure extraction of domesticated *Artemisia absinthium* against Meloidogyne javanica, Crop. Prot. 94 (2017) 33-37

[25] J.L. Marqués, G. Della Porta, E. Reverchon, J.A.R. Renuncio, A.M. Mainar, Supercritical antisolvent extraction of antioxidants from grape seeds after vinification, J. Supercrit. Fluid 82 (2013) 238-243

[26] L. Martín, A. M. Mainar, A. González-Coloma, J. Burillo, J.S. Urieta, Supercritical fluid extraction of wormwood (*Artemisia absinthium* L.), J. Supercrit. Fluid 56 (2011) 64-71

[27] A. González-Coloma, L. Martín, A. M. Mainar, J. S. Urieta, B. M. Fraga, V. Rodríguez-Vallejo, C. E. Díaz, Supercritical extraction and supercritical antisolvent fractionation of natural products from plant material: comparative results on *Persea indica,* Phytochem. Rev. 11(4) (2012) 433-446

[28] J. T. Paula, I. M. O. Sousa, M. A. Foglio, F. A. Cabral, Selective fractionation of extracts of *Arrabidaea chica* Verlot using supercritical carbon dioxide as antisolvent, J. Supercrit. Fluid 133 (2018) 9-16

[29] L. Baldino, G. Della Porta, L. S. Osseo, E. Reverchon, R. Adami, Concentrated oleuropein powder from olive leaves using alcoholic extraction and supercritical CO_2 assisted extraction, J. Supercrit. Fluid 133 (2018) 65-69

[30] Y. M. Monroy, R. A.F. Rodrigues, M. V.N. Rodrigues, F. A. Cabral, Fractionation of ethanolic and hydroalcoholic extracts of green propolis using supercritical carbon dioxide as an anti-solvent to obtain artepillin rich extract, J. Supercrit. Fluid 168 (2018) 167-173

[31] L. Lőrincza, Á. Tótha, L. Kondora, O. Kérib, J. Madarászb, E. Vargac, E. Székelya, Gas antisolvent fractionation based optical resolution of ibuprofen with enantiopure phenylglycinol, J CO_2 Util, 27 (2018) 493-499

[32] A.S.A.E. Standards, Method of determining and expressing fineness of feed materials by sieving, ASAE S319.3 (1997) 547